

Experimental Indication of Existence of Extra Light-Vector Mesons $\omega'(1.3)$ and $\rho'(1.3)$

Toshihiko KOMADA

*Department of Engineering Science, Junior College Funabashi Campus,
Nihon University, Funabashi 274-8501, Japan*

Mass distributions of $\pi^+\pi^-\pi^0$ and $\omega\pi^0$ systems in the e^+e^- annihilation obtained by the several experiments are analyzed. We obtain indication of light-vector mesons $\omega'(1.3)$ and $\rho'(1.3)$ in the lower mass region. Those states are expected to exist in the $\tilde{U}(12)$ -classification scheme.

§1. Introduction

Recently the $\tilde{U}(12)$ level-classification scheme of hadrons¹⁾ has been proposed, which is a covariant generalization of non-relativistic scheme based on $SU(6)_{SF}$. In the $\tilde{U}(12)$ -classification scheme a new type of relativistic states, called chiral states, which have no correspondents in the non-relativistic scheme, are expected to exist in lower mass region for light quark systems. Especially the extra vector meson nonet is predicted in the ground S-wave state of $(q\bar{q})$ system.

On the other hand, experimentally it is noted that the recent data of 3π and $\omega\pi^0$ states in e^+e^- annihilation show a hint for an extra state $\omega(1200)$.²⁾ The studies in hadroproduction and others have shown indication of low mass extra states.³⁾ Further studies on their existence will be interesting.

In this work we re-analyzed mass spectra of $\pi^+\pi^-\pi^0$ ^{4),5)} and $\omega\pi^0$ ^{6),7),8)} in e^+e^- annihilation, and have obtained indication of a low mass ω and a low mass ρ in respective channels around 1.3 GeV. These seem to be ground-state chiralons (pure chiral state) expected in the $\tilde{U}(12)$ scheme.⁹⁾

§2. Analysis of the mass spectrum of $\pi^+\pi^-\pi^0$ and indication of extra vector meson $\omega'(1.3)$

In this work we are going to reanalyze the combined mass spectrum of the $\pi^+\pi^-\pi^0$ data in the e^+e^- annihilation obtained by SND⁴⁾ and by BABAR.⁵⁾ The former presents higher statistics data at the lower mass region and the latter covers the whole mass region interested as shown in Fig. 1. The DM2 data¹⁰⁾ which were included in our previous analysis¹¹⁾ are not used in the present analysis since they seem to show different behaviors from those of BABAR depending on a bias factor for cross sections.

The relevant process $e^+e^- \rightarrow \pi^+\pi^-\pi^0$ is, applying the vector meson dominance model (VMD), considered to occur dominantly through intermediate production of

vector mesons “V” as that $e^+e^- \rightarrow \gamma \rightarrow “V” \rightarrow \rho\pi \rightarrow 3\pi$. The analysis results obtained by SND and by BABAR show vectors, $\omega(782)$, $\phi(1020)$, $\omega(1420)$ and $\omega(1650)$, but no $\omega(1200)$. The width parameter for $\omega(1420)$ is obtained to be rather wider in each analysis, as shown in Table I. There recognized, however, a huge event accumulation exists around 1.3 GeV in the 3π mass spectrum. It may be naturally interpreted to correspond to the $\omega(1200)$, which was pointed out in ref. 2), rather than $\omega(1420)$.

In order to make clear the situation on the existence of $\omega(1200)$, a possible contribution of a low mass state $\omega'(1.3)$ is considered explicitly in the present work in addition to the higher vector mesons, $\omega(1420)$ and $\omega(1650)$.

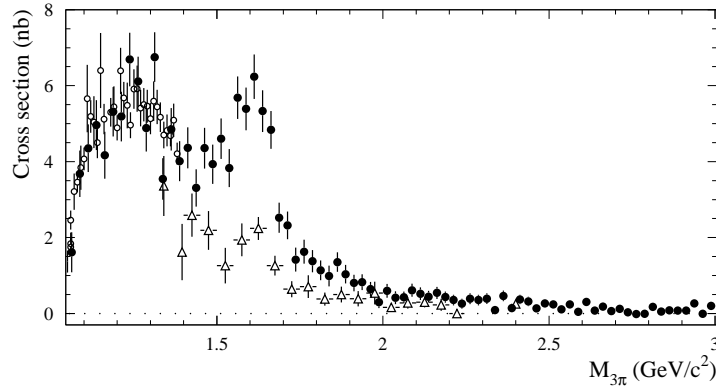


Fig. 1. The $e^+e^- \rightarrow \pi^+\pi^-\pi^0$ cross section by BABAR⁵⁾ (filled circles), by SND⁴⁾ (open circles), and by DM2⁸⁾ (open triangles).

Table I. Masses and widths of $\omega(1420)$ in $e^+e^- \rightarrow \pi^+\pi^-\pi^0$ are listed.

| $\omega(1420)$ | M (MeV) | Γ (MeV) |
|---------------------|-----------------------|-----------------------------|
| BABAR ⁵⁾ | $1350 \pm 20 \pm 20$ | $450 \pm 70 \pm 70$ |
| SND ⁴⁾ | $1400 \pm 50 \pm 130$ | $870_{-300}^{+500} \pm 450$ |

2.1. Method of analysis

First we give general effective Lagrangians, which concern on our relevant processes given in Fig. 2, as

$$\begin{aligned}
\mathcal{L}_{e^+e^-\gamma} &= ie\bar{\psi}_e\gamma_\mu\psi_e\mathbf{A}_\mu, \\
\mathcal{L}_{\gamma V} &= \left(\frac{em_\omega^2}{3f_\omega}\omega_\mu - \frac{\sqrt{2}em_\phi^2}{3f_\phi}\phi_\mu\right)A_\mu, \\
&\quad (“V” = \omega(782), \phi(1020), \omega^{(1)}, \omega^{(2)} \text{ and } \omega^{(3)}), \\
\mathcal{L}_{\omega\rho\pi} &= g_{\omega\rho\pi}\varepsilon_{\mu\nu\lambda\kappa}\partial_\mu\omega_\nu\partial_\lambda\rho_\kappa\cdot\pi, \\
\mathcal{L}_{\phi\rho\pi} &= g_{\phi\rho\pi}\varepsilon_{\mu\nu\lambda\kappa}\partial_\mu\phi_\nu\partial_\lambda\rho_\kappa\cdot\pi, \\
\mathcal{L}_{\rho\pi\pi} &= -f_{\rho\pi\pi}\rho_\mu(\pi\times\partial_\mu\pi),
\end{aligned} \tag{2.1}$$

where f_V being coupling constant of decay interaction for “V” $\rightarrow e^+e^-$. The cross section for relevant process is given as

$$\sigma(s) = \frac{4\pi\alpha^2}{s^{\frac{3}{2}}} \left| A_\omega \frac{m_\omega^2 \sqrt{F_\omega(s)}}{m_\omega^2 - s - im_\omega \Gamma_\omega} + A_\phi \frac{m_\phi^2 \sqrt{F_\phi(s)}}{m_\phi^2 - s - im_\phi \Gamma_\phi} + \sum_{i=1}^3 A_i \frac{m_{\omega^{(i)}}^2 \sqrt{F_{\omega^{(i)}}(s)}}{m_{\omega^{(i)}}^2 - s - im_{\omega^{(i)}} \Gamma_{\omega^{(i)}}} \right|^2 4\pi \Gamma(s), \quad (2.2)$$

where $\omega^{(1)}, \omega^{(2)}$ and $\omega^{(3)}$ denote a low mass and two higher mass vector states above 1 GeV.

In Eq. (2.2) we have introduced the form factor F given as

$$F_R(s) = \frac{2m_R^2}{m_R^2 + s}, \quad (2.3)$$

and A_i 's are the fitting parameters, while the values of A_ω and A_ϕ has been estimated from the relevant low mass data.

$$\Gamma(s) = \frac{f_{\rho\pi\pi}^2}{3 \cdot 16\pi^3} \int_{2m_\pi}^{\sqrt{s}-m_\pi} d\sqrt{s_{12}} |\mathbf{q}|^3 |\mathbf{p}_1|^3 \cdot \int_{-1}^1 d(\cos\theta) \sin^2\theta |\mathcal{F}_{\rho\pi\pi}|^2, \\ \mathcal{F}_{\rho\pi\pi} = \frac{\sqrt{F_\rho(s_{12})}}{m_\rho^2 - s_{12} - im_\rho \Gamma_\rho} + \frac{\sqrt{F_\rho(s_{23})}}{m_\rho^2 - s_{23} - im_\rho \Gamma_\rho} + \frac{\sqrt{F_\rho(s_{31})}}{m_\rho^2 - s_{31} - im_\rho \Gamma_\rho}, \\ (f_{\rho\pi\pi}^2 = “1”), \quad (2.4)$$

where s_{ij} 's are invariant mass of three possible contribution of π^+ , π^- and π^0 . θ is angle between ρ and π in ω at rest. \mathbf{q} and \mathbf{p}_1 is 3-momentum of \mathbf{p}_{π_3} at $\pi_1\pi_2\pi_3$ C.M.S. and of \mathbf{p}_{π_1} at $\pi_1\pi_2$ C.M.S., respectively. The value of common factor of the cross section, $f_{\rho\pi\pi}^2$, is irrelevant to our analysis.

There are two contrastive structures in 3π mass spectrum of $e^+e^- \rightarrow \pi^+\pi^-\pi^0$ below 2 GeV. One is below 1 GeV region and the other is above 1 GeV region. The

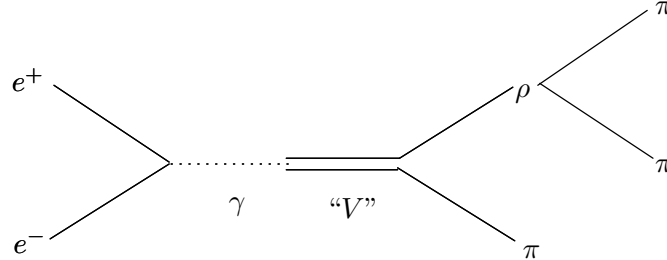


Fig. 2. Diagram of $e^+e^- \rightarrow \gamma \rightarrow \pi^+\pi^-\pi^0$.

former region has two clear and huge peaks coming from contributions from $\omega(782)$ and $\phi(1020)$ as shown in Fig. 3a), while the latter shows some complex structures (which are relevant to the present work) as shown in Fig. 1 and Fig. 3b).

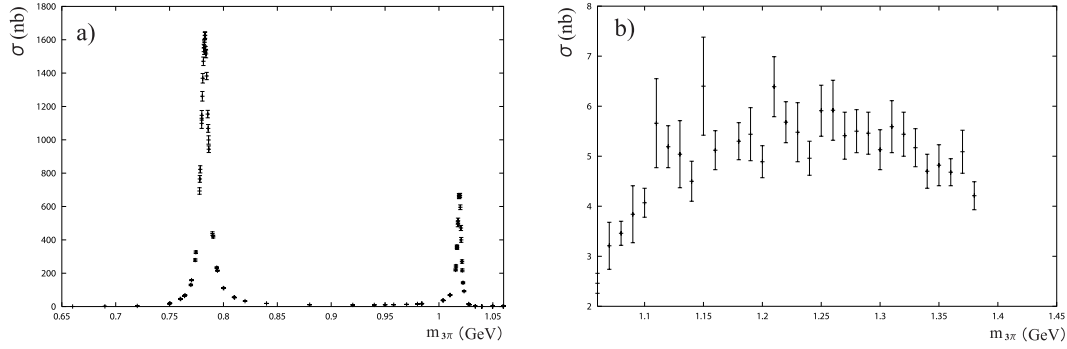


Fig. 3. The $e^+e^- \rightarrow \pi^+\pi^-\pi^0$ cross section by SND,⁴⁾ a) below 1 GeV region c) above 1 GeV region.

Before 3π mass spectrum of $e^+e^- \rightarrow \pi^+\pi^-\pi^0$ in the energy region from 1.06 to 2.0 GeV by BABAR and by SND are analyzed, the parameters A_ω and A_ϕ of $\omega(782)$ and $\phi(1020)$ in Eq. (2.2) are fixed by the analysis of the spectrum below 1 GeV. Then these values^{*)} of parameter A_ω and A_ϕ are applied in the analysis of the data above 1 GeV.

2.2. Results of analysis

The 3π mass spectrum of $e^+e^- \rightarrow \pi^+\pi^-\pi^0$ in the energy region from 1.06 to 2.0 GeV are used in the analyses of the following three cases.

In the fitting of the first case, two resonances are considered above 1 GeV region. The values of mass and width of $\omega^{(1)}$ and $\omega^{(2)}$, corresponding to $\omega(1420)$ and $\omega(1650)$, are restricted to be consistent with PDG tables.¹²⁾ In this case, the experimental data are not well reproduced, especially below 1.5 GeV region.

In the second case, two resonances are considered above 1 GeV region. The values of mass and width of $\omega^{(2)}$, corresponding to $\omega(1650)$, are restricted to be consistent with PDG tables,¹²⁾ while the parameters of $\omega^{(1)}$ are not restricted. In this case, the experimental data are well reproduced, although obtained values of mass and width of $\omega^{(1)}$ are lower and wider, respectively, compared with $\omega(1420)$ of PDG values.

In the third case, three resonances are considered above 1 GeV region. The values of mass and width of $\omega^{(2)}$ and $\omega^{(3)}$, corresponding to $\omega(1420)$ and $\omega(1650)$, are restricted to be consistent with PDG tables,¹²⁾ while the parameters of $\omega^{(1)}$, supposed to be corresponding to the extra $\omega'(1.3)$, are not restricted. In this case, the experimental data are well reproduced. The contributions of $\omega^{(1)}$ and $\omega^{(3)}$ are large, while the contribution of $\omega^{(2)}$ is very small.

All the results of three cases are shown in Fig. 4, Fig. 5, and Fig. 6a). In addition mass and width scan on $\omega^{(1)}$ for the third case are shown in Fig. 6b). The obtained values of parameters and $\chi^2/N_{d.o.f.}$ in the three cases are listed in Table II.

The almost same values of $\chi^2/N_{d.o.f.}$ are obtained in the second and the third case. This reflect that the contribution of $\omega(1420)$ in the third case is very small,

*) $A_\omega = 0.64$, $A_\phi = -0.041$.

and implies that a dominant contribution of $\omega'(1.3)$ in this case is replaced by that of $\omega(1420)$ in the second case.

The result of fitting of the third case is improved by about 19σ compared with the first case, indicating the existence of the low mass extra vector meson $\omega'(1.3)$ in addition to the two higher states $\omega(1420)$ and $\omega(1650)$.

It is noted that the obtained values of $m_{\omega(1)}$ in the second and third case are slightly larger than the center of accumulation, around 1.25 GeV, in 3π mass spectrum as shown in Fig. 1 and Fig. 3b). It is due to interference effect among $\omega(782)$, $\phi(1020)$, and $\omega'(1.3)$.

Table II. The obtained values of parameters and $\chi^2/N_{d.o.f.}$.

| Two resonance analysis | | | |
|--------------------------|-------------------------------------|--------------------|--------------------|
| | $\omega^{(1)}$ | $\omega^{(2)}$ | |
| Case 1 | $\chi^2/N_{d.o.f.} = 442/64 = 6.91$ | | |
| $m(\text{MeV})$ | 1400^\dagger | 1626 ± 5 | |
| $\Gamma(\text{MeV})$ | 250^\dagger | 280^\ddagger | |
| A | -0.039 ± 0.002 | -0.058 ± 0.002 | |
| Case 2 | $\chi^2/N_{d.o.f.} = 76/64 = 1.19$ | | |
| $m(\text{MeV})$ | 1303 ± 10 | 1601 ± 5 | |
| $\Gamma(\text{MeV})$ | 641 ± 49 | 180^\ddagger | |
| A | -0.191 ± 0.018 | -0.027 ± 0.003 | |
| Three resonance analysis | | | |
| | $\omega^{(1)}$ | $\omega^{(2)}$ | $\omega^{(3)}$ |
| Case 3 | $\chi^2/N_{d.o.f.} = 73/61 = 1.19$ | | |
| $m(\text{MeV})$ | 1346 ± 26 | 1450^\dagger | 1597 ± 6 |
| $\Gamma(\text{MeV})$ | 639 ± 42 | 250^\dagger | 180^\ddagger |
| A | -0.207 ± 0.015 | 0.015 ± 0.010 | -0.026 ± 0.003 |

† Bound for upper limit which is set to be consistent with PDG tables.

‡ Bound for lower limit which is set to be consistent with PDG tables.

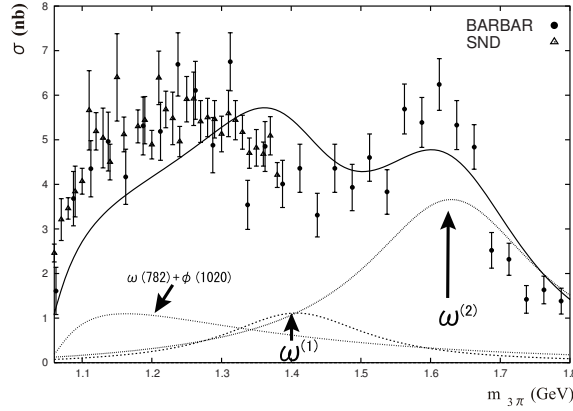


Fig. 4. Results of the analysis of the first case (fit with $\omega^{(1)}$, $\omega^{(2)}$) on 3π mass spectrum of $e^+e^- \rightarrow \pi^+\pi^-\pi^0$. Data are from SND⁴⁾ and BABAR.⁵⁾ Solid line is fitted curve. Dotted lines represent the contribution of each amplitude.

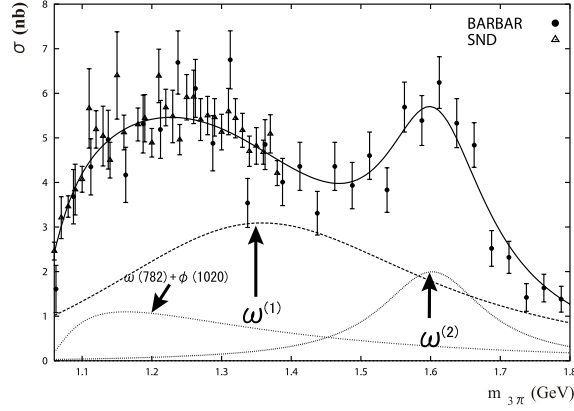


Fig. 5. Results of the analysis of the second case (fit with $\omega^{(1)}$, $\omega^{(2)}$) on 3π mass spectrum of $e^+e^- \rightarrow \pi^+\pi^-\pi^0$. Data are from SND⁴⁾ and BABAR.⁵⁾ Solid line is fitted curve. Dotted lines represent the contribution of each amplitude.

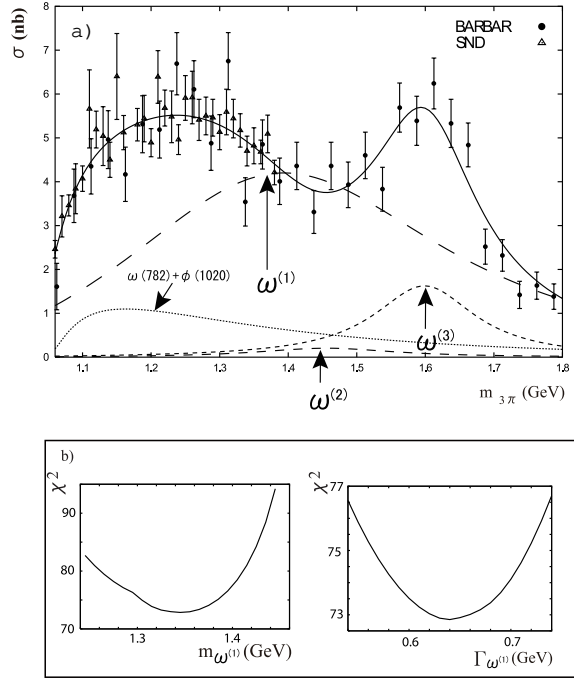


Fig. 6. a) Results of the analysis of the third case (fit with $\omega^{(1)}$, $\omega^{(2)}$, $\omega^{(3)}$) on 3π mass spectrum of $e^+e^- \rightarrow \pi^+\pi^-\pi^0$. b) Mass and width scan on $\omega^{(1)}$ for the third case. Data are from SND⁴⁾ and BABAR.⁵⁾ Solid line is fitted curve. Dotted lines represent the contribution of each amplitude.

§3. Analysis of the mass spectrum of $\omega\pi^0$ and indication of extra vector meson $\rho'(1.3)$

In this work we are also going to reanalyze the combined mass spectrum of $\omega\pi^0$ data in e^+e^- annihilation obtained by CMD-2,⁶⁾ by SND⁷⁾ and by DM2.⁸⁾ The CLEO data¹³⁾ which were included in our previous analysis¹¹⁾ are not used in the present analysis to make the situation simple for analysis since the CLEO data were obtained from $\tau \rightarrow \omega\pi^0$ which is the different process from $e^+e^- \rightarrow \omega\pi^0$.

The process is also, applying the VMD, considered to occur dominantly through intermediate production of vector mesons “V” as that $e^+e^- \rightarrow \gamma \rightarrow \text{“V”} \rightarrow \omega\pi^0$. The analysis results obtained by CMD-2 show vectors, $\rho(770)$, $\rho(1450)$ and $\rho(1700)$, while mass and width values of the $\rho(1450)$ are scattered in each study.¹²⁾ There recognized, however, a huge event accumulation exists around 1.3 GeV in the $\omega\pi^0$ mass spectrum. It may be naturally interpreted to correspond to the $\rho'(1.3)$ with mass around 1.3 GeV which has lower mass than $\rho(1450)$. Actually the existence of $\rho'(1.3)$ was pointed out by several experimental group^{14),15)} and in review articles.^{12),3)}

In order to make clear the situation on the existence of extra light-vector meson, a possible contribution of $\rho'(1.3)$ is considered explicitly in the present work in addition to the higher vector mesons, $\rho(1450)$ and $\rho(1700)$.

3.1. Method of analysis

Effective Lagrangians, which concern on our relevant processes given in Fig. 7, are given as

$$\begin{aligned}\mathcal{L}_{e^+e^-\gamma} &= ie\bar{\psi}_e\gamma_\mu\psi_e A_\mu, \\ \mathcal{L}_{\gamma V} &= \gamma_V V_\mu^3 A_\mu, \quad (\gamma_V = \frac{em_V^2}{f_V}) \\ \mathcal{L}_{V\omega\pi} &= g_{V\omega\pi}\epsilon_{\mu\nu\lambda\kappa}\partial_\mu\mathbf{V}_\nu\partial_\lambda\omega_\kappa\pi \\ &\quad (\text{“V”} = \rho(770), \rho^{(1)}, \rho^{(2)}, \text{ and } \rho^{(3)}),\end{aligned}\quad (3.1)$$

where f_V being coupling constant of decay interaction for “V” $\rightarrow e^+e^-$. $\rho^{(1)}$, $\rho^{(2)}$ and $\rho^{(3)}$ denote a low mass and two higher mass vector states. The cross section is given as

$$\sigma_0(s) = \frac{4\pi\alpha^2}{s^{\frac{3}{2}}} \left(\frac{g_{\rho\omega\pi}}{f_\rho} \right)^2 \left| \frac{m_\rho^2 \sqrt{F_\rho(s)}}{D_\rho(s)} + \sum_{i=1}^3 A_i \frac{m_{\rho^{(i)}}^2 \sqrt{F_{\rho^{(i)}}(s)}}{m_{\rho^{(i)}}^2 - s - im_{\rho^{(i)}}\Gamma_{\rho^{(i)}}} \right|^2 P_f(s), \quad (3.2)$$

where

$$F_R(s) = \frac{2m_R^2}{m_R^2 + s}, \quad P_f(s) = \frac{1}{3} |\mathbf{p}_\omega(s)|^3 \cdot B_{\omega \rightarrow \pi^0 \gamma}. \quad (3.3)$$

$\mathbf{p}_\omega(s)$ is three momentum of ω in ρ at rest. $B_{\omega \rightarrow \pi^0 \gamma}$ is branching ratio of $\omega \rightarrow \pi^0 \gamma$ to be 0.085 ± 0.005 . Coupling constants are estimated by VMD using experimental values to be $f_\rho = 5.04$ and $g_{\rho\omega\pi} = 12.47$. A_i ’s are the fitting parameters.

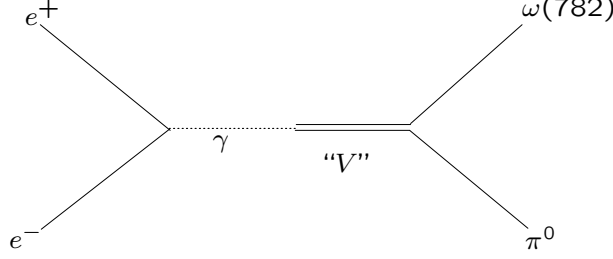


Fig. 7. Diagram of $e^+e^- \rightarrow \gamma \rightarrow \omega\pi^0$.

3.2. Results of analysis

The $\omega\pi$ mass spectrum of $e^+e^- \rightarrow \omega\pi^0$ below 2.2 GeV are used in the analyses of following three cases in parallel with the analyses on $\pi^+\pi^-\pi^0$.

In the fitting of the first case, two resonances are considered above 1 GeV region. The values of mass and width of $\rho^{(1)}$ and $\rho^{(2)}$, corresponding to $\rho(1450)$ and $\rho(1700)$, are restricted to be consistent with PDG tables.¹²⁾ In this case, the experimental data are not well reproduced, especially below 1.4 GeV region.

In the second case, two resonances are considered above 1 GeV region. The values of mass and width of $\rho^{(2)}$, corresponding to $\rho(1700)$, are restricted to be consistent with PDG tables,¹²⁾ while the parameters of $\rho^{(1)}$ are not restricted. In this case, the experimental data are well reproduced, although obtained values of mass and width of $\rho^{(1)}$ are lower and wider, respectively, compared with those of $\rho(1450)$ of PDG values.

In the third case, three resonances are considered above 1 GeV region. The values of mass and width of $\rho^{(2)}$ and $\rho^{(3)}$, corresponding to $\rho(1450)$ and $\rho(1700)$, are restricted to be consistent with PDG tables,¹²⁾ respectively, while the parameters of $\rho^{(1)}$, supposed to be corresponding to the extra $\rho'(1.3)$, are not restricted. In this case, the experimental data are well reproduced. The contribution from $\rho^{(1)}$ is large, while those of $\rho^{(2)}$ and $\rho^{(3)}$ are very small comparing to that of $\rho^{(1)}$.

All the results of three cases are shown in Fig. 8, Fig. 9, and Fig. 10a). In addition mass and width scan on $\rho^{(1)}$ for the third case are shown in Fig. 10b). The obtained values of parameters and $\chi^2/N_{d.o.f.}$ in the three cases are listed in Table III. The result of fitting of the third case is improved by about 24σ compared with the first case, indicating the existence of the low mass extra vector meson $\rho'(1.3)$ in addition to two higher state $\rho(1450)$ and $\rho(1700)$.

It may be noted that the CMD-2 data and SND data cover below 1.4 GeV of $\omega\pi$ mass spectrum, while the DM2 data covers above 1.4 GeV. The combined data of two regions below and above 1.4 GeV are used*) in the present analysis. That the DM2 data show their cross section values rather suppressed would result less contribution of $\rho(1700)$ than those of $\rho'(1.3)$ or $\rho(1450)$.

*) A bias factor 1.18 is applied on DM2 data by CMD-2.

Table III. The obtained values of parameters and $\chi^2/N_{d.o.f.}$.

| Two resonance analysis | | | |
|--------------------------|-------------------------------------|--------------------|-------------------|
| | $\rho^{(1)}$ | $\rho^{(2)}$ | |
| Case 1 | $\chi^2/N_{d.o.f.} = 801/60 = 13.4$ | | |
| $m(\text{MeV})$ | 1440^\ddagger | 1700 | |
| $\Gamma(\text{MeV})$ | 385 ± 13 | 240 | |
| A | -0.253 ± 0.009 | 0.008 ± 0.003 | |
| Case 2 | $\chi^2/N_{d.o.f.} = 235/60 = 3.91$ | | |
| $m(\text{MeV})$ | 1251 ± 11 | 1700 | |
| $\Gamma(\text{MeV})$ | 563 ± 19 | 240 | |
| A | -0.545 ± 0.031 | 0.016 ± 0.003 | |
| Three resonance analysis | | | |
| | $\rho^{(1)}$ | $\rho^{(2)}$ | $\rho^{(3)}$ |
| Case 3 | $\chi^2/N_{d.o.f.} = 231/55 = 4.19$ | | |
| $m(\text{MeV})$ | 1247 ± 9 | 1440^\ddagger | 1700 |
| $\Gamma(\text{MeV})$ | 506 ± 30 | 340^\ddagger | 240 |
| A | -0.435 ± 0.053 | -0.044 ± 0.020 | 0.012 ± 0.003 |

[†] Bound for upper limit which is set to be consistent with PDG tables.

[‡] Bound for lower limit which is set to be consistent with PDG tables.

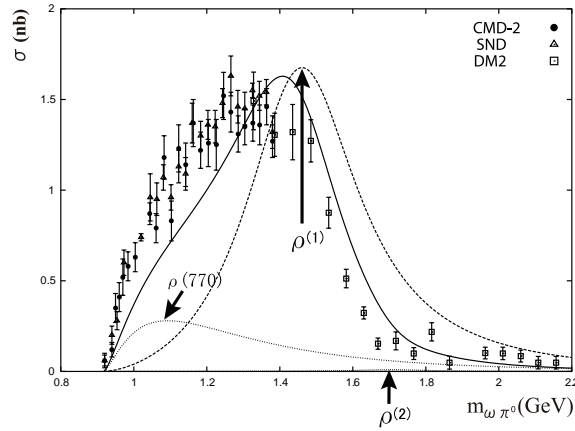


Fig. 8. Results of the analysis of the first case (fit with $\rho^{(1)}$, $\rho^{(2)}$) on $\omega\pi^0$ mass spectrum of $e^+e^- \rightarrow \omega\pi^0$. Data are from CMD-2,⁶⁾ SND,⁷⁾ and DM2.⁸⁾ Solid line is fitted curve. Dotted lines represent the contribution of each amplitude.

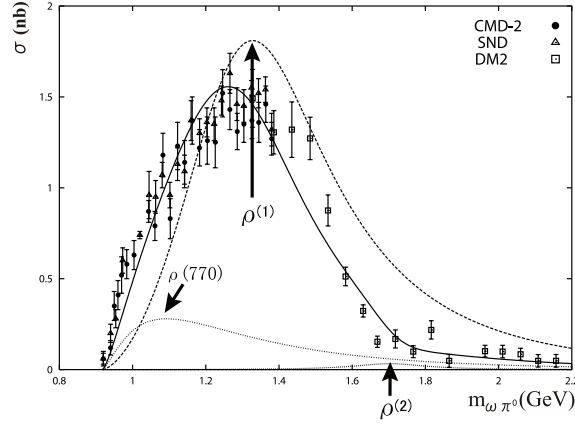


Fig. 9. Results of the analysis of the second case (fit with $\rho^{(1)}$, $\rho^{(2)}$) on $\omega\pi^0$ mass spectrum of $e^+e^- \rightarrow \omega\pi^0$. Data are from CMD-2,⁶⁾ SND,⁷⁾ and DM2.⁸⁾ Solid line is fitted curve. Dotted lines represent the contribution of each amplitude.

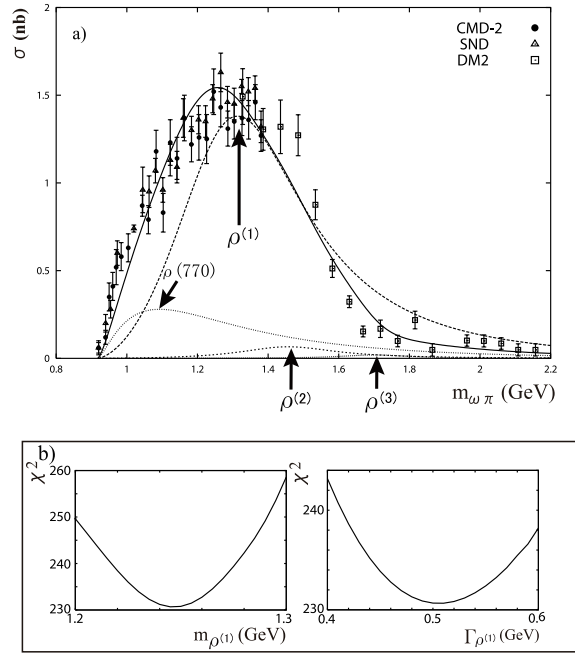


Fig. 10. a) Results of the analysis of the third case (fit with $\rho^{(1)}$, $\rho^{(2)}$, $\rho^{(3)}$) on $\omega\pi^0$ mass spectrum of $e^+e^- \rightarrow \omega\pi^0$. b) Mass and width scan on $\rho^{(1)}$ for the third case. Data are from CMD-2,⁶⁾ SND,⁷⁾ and DM2.⁸⁾ Solid line is fitted curve. Dotted lines represent the contribution of each amplitude.

§4. Concluding remarks

Through the present analyses on the mass spectra of $\pi^+\pi^-\pi^0$ and of $\omega\pi^0$ in e^+e^- annihilation we have shown some indication of low mass vector mesons $\omega'(1.3)$ and $\rho'(1.3)$, respectively. The obtained values of masses and widths are

$$\begin{aligned} m_{\omega'(1.3)} &= 1346 \pm 26 \text{ (MeV)}, \\ \Gamma_{\omega'(1.3)} &= 639 \pm 42 \text{ (MeV)}, \\ m_{\rho'(1.3)} &= 1247 \pm 9 \text{ (MeV)}, \\ \Gamma_{\rho'(1.3)} &= 506 \pm 30 \text{ (MeV)}. \end{aligned}$$

The results are still preliminary, as the used data are combined one coming from different experiments performed in different mass regions. However, we expect that the main feature on mass spectra may be considered to be maintained, independently of a bias factor.

Accordingly, we may conclude that the extra-vector mesons $\omega'(1.3)$ and $\rho'(1.3)$ are necessary to explain the mass spectra. In each result of the third case in Table II and Table III, the contributions of $\omega(1420)$ and $\rho(1450)$ are very small compared with those of $\omega'(1.3)$ and $\rho'(1.3)$, respectively.

The present results seem to be consistent with the expectation of the $\tilde{U}(12)$ -scheme. In this scheme $\omega'(1.3)$ and $\rho'(1.3)$ are assigned as S-wave chiral states⁹⁾ while $\omega(1420)$ and $\rho(1450)$ are assigned as P-wave states. Accordingly the contributions of $\omega(1420)$ and $\rho(1450)$ are expected to be very small compared with those of $\omega'(1.3)$ and $\rho'(1.3)$, respectively, reflecting the strength at the origin of their wave functions, $|\psi_P(0)|^2 \simeq 0$ and $|\psi_S(0)|^2 \simeq 1$.

Further studies are expected to confirm the existence of the low mass extra vector mesons $\omega'(1.3)$ and $\rho'(1.3)$: It will be a very important problem for hadron spectroscopy.

Acknowledgements

We would like to express our sincere appreciation to Dr. M. Ishida who initiated this work and gave us helpful and crucial suggestions during the work. We deeply appreciate Prof. K. Yamada, Prof. K. Takamatsu, and Prof. I. Yamauchi who gave us useful and crucial discussions and information. We also thank Prof. S. Ishida, Prof. T. Tsuru, Dr. T. Maeda, and Prof. M. Oda for useful discussions. This work is supported by Nihon University Individual Research Grant for (2005).

References

- 1) S. Ishida, M. Ishida and T. Maeda, Prog. Theor. Phys. **104** (2000) 785; S. Ishida and M.Y. Ishida, Phys. Lett. **B539** (2002) 249-256.
- 2) M.N. Achasov et al. (SND Collaboration), Phys. Lett. **B462** (1999) 365-370.
- 3) A. Donnachie and Yu.S. Karashnikova, Proc. 9th Hadron Conf. 2001, AIP Conf. Proc. **619** (2002) 5; A. Donnachie, Phys. Rept. **403-404** (2004) 281-301.
- 4) M.N. Achasov et al. (SND Collaboration), Phys. Rev. **D68** (2003) 052006.
- 5) B. Aubert et al. (BABAR Collaboration), Phys. Rev. **D70** (2004) 072004.
- 6) R. R. Akhmetshin et al. (CMD-2 Collaboration), Phys. Lett. **B562** (2003) 173.
- 7) M.N. Achasov et al. (SND Collaboration), Phys. Lett. **B486** (2000) 29.

- 8) Nuclear Physics B (Proc. Suppi.) **21** (1991) 111-117.
- 9) K. Yamada, in these proceedings.
- 10) A. Antonelli et al. (DM2 Collaboration), Z. Phys. **C56** (1992) 15.
- 11) T. Komada, AIP Conf. Proc. **814** (2006) 458.
- 12) Particle Data Group, S. Eidelman et al., Phys. Lett. **B592** (2004) 1.
- 13) K. W. Edwards et al. (CLEO Collaboration), Phys. Rev. **D61** (2000) 072003.
- 14) D. Aston et al. (LASS Collaboration), SLAC-PUB-5606 (1994).
- 15) A. Bertin et al. (OBELIX Collaboration) Phys. Lett. **B414** (1997) 220.